Journal of Computer-Aided Molecular Design **18:** 651–664, 2004.
DOI 10.1007/s10822-004-6259-0

Subunit rotation models activation of serotonin 5-HT_{3AB} receptors by agonists

Gábor Maksay[†], Miklós Simonyi & Zsolt Bikádi[†,*]
Molecular Pharmacology Group, Institute for Biomolecular Chemistry, Chemical Research Centre, Hungarian Academy of Sciences, P.O. Box 17, 1525 Budapest, Hungary

Received 29 June 2004; accepted in revised form 13 November 2004

Key words: docking of agonists, homology modelling, hydrogen bond analysis, 5-hydroxytryptamine$_3$ receptors, *m*-chlorophenylbiguanide, subunit rotation

Summary

The N-terminal extracellular regions of heterooligomeric 3AB-type human 5-hydroxytryptamine receptors (5-HT_{3AB}R) were modelled based on the crystal structure of snail acetylcholine binding protein AChBP. Stepwise rotation of subunit A by 5° was performed between −10° and 15° to mimic agonist binding and receptor activation. Anticlockwise rotation reduced the size of the binding cavity in interface AB and reorganised the network of hydrogen bonds along the interface. AB subunit dimers with different rotations were applied for docking of ligands with different efficacies: 5-HT, *m*-chlorophenylbiguanide, SR 57227, quinolinyl piperazine and lerisetron derivatives. All ligands were docked into the dimer with −10° rotation representing ligand-free, open binding cavities similarly, without pharmacological discrimination. Their ammonium ions were in hydrogen bonding distance to the backbone carbonyl of W183. Anticlockwise rotation and contraction of the binding cavity led to distinctive docking interactions of agonists with E129 and cation–π interactions of their ammonium ions. Side chains of several further amino acids participating in docking (Y143, Y153, Y234 and E236) are in agreement with the effects of point mutations in the binding loops. Our model postulates that 5-HT binds to W183 in a hydrophobic cleft as well as to E236 in a hydrophilic vestibule. Then it elicits anticlockwise rotation to draw in loop C via π–cation–π interactions of its ammonium ion with W183 and Y234. Finally, closure of the binding cavity might end in rebinding of 5-HT to E129 in the hydrophilic vestibule.

Abbreviations: AChBP – acetylcholine binding protein; AMBER – assisted model building with energy refinement; AQPA – arylquinolinyl piperazine; BQPA – bicyclooctano-quinolinyl piperazine; CPBG – *m*-chlorophenylbiguanide; $GABA_A$ – γ-aminobutyric $acid_A$; 5-HT – 5-hydroxytryptamine (serotonin); LGA – Lamarckian genetic algorithm; PDB – protein data bank; RMSD – relative mean standard deviation; SR 57227 – 4-amino-(6-chloro-2-pyridyl)-1-piperidine HCl; TM – transmembrane.

Introduction

Agonists elicit efficacy-dependent rotations of AMPA-type glutamate receptors and closure of the binding cavity [1]. Activation of the Cys-loop superfamily of ionotropic receptors has been conceived from electron microscopic images of nicotinic receptors [2]. Clockwise rotation of the pore-facing parts of the transmembrane (TM) regions of nicotinic receptor subunits results in more compact structures [3]. 5-Hydroxytryptamine type 3 receptors (5-HT_3R) are the only serotonin

[†]Authors with equal contribution to the manuscript.
*To whom correspondence should be addressed. Tel: 361-438-0411; Fax: 361-325-7554; E-mail: bikadi@chemres.hu

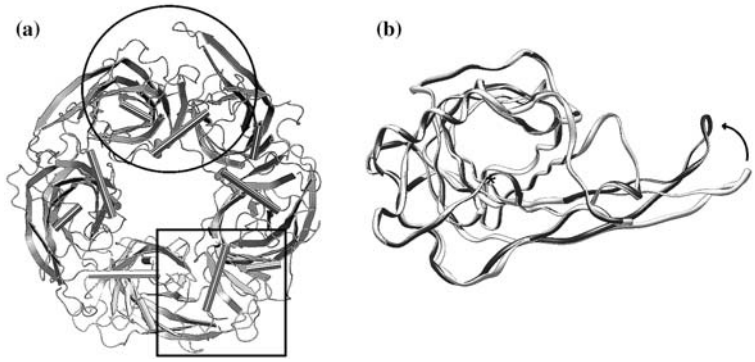

Figure 1. (a) X-ray structures of an AChBP pentamer with open (encircled) and closed (squared) binding clefts. One closed binding cavity harbours co-crystallized carbamylcholine (not shown). Taken from RCSB Protein Bank entry number 1UV6 [12]. (b) The subunits with open (light) and closed (dark) binding clefts overlap except for the protruding loop C. The conformational change elicited by agonist binding is modelled by anticlockwise rotation of subunit A around the perpendicular axis labelled x.

receptors of ionotropic kind. They belong to the Cys-loop superfamily of transmitter-gated ion channels together with nicotinic acetylcholine receptors, A type γ-aminobutyric acid ($GABA_A$) and glycine receptors [4]. 5-HT_3Rs have been implicated in anxiety, psychosis, depression, antinociception, cognition and emesis [5]. 5-HT_3R antagonists have been used as antiemetic drugs in cancer therapy. Five 5-HT_3R subunits form a cation channel [6]. The principal subunits A function as homopentamers mainly in the central nervous system, while the majority of 5-HT_3Rs are heteropentamers of subunits A and B in the periphery [7]. The genes of human 5-HT_3R C, D and E subunits have also been described recently [8, 9].

Electron microscopic images of basal and activated nicotinic acetylcholine receptors form the basis of our understanding of the structure and activation of the Cys-loop superfamily of ionotropic receptors [2]. However, these low-resolution images cannot elucidate the binding sites of ligands. A snail acetylcholine binding protein (AChBP) shows 22–30% sequence homology with the N-terminal regions of the Cys-loop family [10]. However, this low homology can result in about 80% accuracy to estimate secondary structures [11]. Consequently, the crystal structure of AChBP has revealed the structural details of the extracellular parts of pentameric channels including binding cavities at subunit interfaces encircled by six binding loops A–F. A high-resolution (2–3 Å) X-ray crystallographic study has been recently published [12] to show the binding interactions of nicotinic agonists in the interfaces of pentameric AChBP (Figure 1a). Binding of agonists can be associated with anticlockwise rotation of loop C. The protruding loop C in ligand-free AChBP turns anticlockwise upon bound agonists and contracts the binding cavity underneath [12] (Figure 1b).

Based on a ligand-bound structure of AChBP, homology modelling has been successfully performed for nicotinic [13], $GABA_A$ [14] and glycine receptors [15]. Furthermore, binding cavities of allosteric modulators have also been modelled such as for benzodiazepines on $GABA_A$ receptors [14] and eserine on $\alpha3\beta4$ neuronal nicotinic receptors [16]. The homopentameric 5-HT_{3A}R, a possible common ancestor of the Cys-loop family [4], has also been homology modelled and used for docking of 5-HT [17] and 5-HT_3R antagonists [18]. Aromatic rings of 5-HT_3R antagonists are intercalated between W183 and Y234 in π–π interactions. A recent review has summarised several residues, which participate in ligand binding and activation of 5-HT_{3A}Rs [19]. Further residues such as tyrosines Y141, Y143 and Y153 in loop E [20, 21], and glutamates E225 and E236 in loop C [22] also contribute to ligand binding. Finally, R246 in the pre-TM 1 region affects channel gating of 5-HT_{3A}Rs [23]. The predictive value of 5-HT_{3A}R modelling has been recently confirmed experimentally with point mutations of Y143, Y153 and Y234 [21, 52]. Moreover, AChBP has been recently fused with the pore domain of 5-HT_{3A}R and only when three loops in AChBP were also changed for the corresponding residues of 5-HT_{3A}Rs did acetylcholine bind and activate the ion channel [53]. Consequently, homology

modelling can be useful in the structural investigation of not only the binding domain but also its interface with the pore region and activation.

Docking of 5-HT to a 5-HT_{3A}R model resulted in seven energetically favourable binding models [17] but it is difficult to tell which interactions are responsible for activation. The amino acids participating in 5-HT docking included several crucial residues, which affect agonist binding and/or gating. However, E129 and F130 in the vestibule of the binding cavity did not seem to participate in 5-HT docking, although they did affect agonist binding and/or gating [24, 25]. It should be noted that the distance of the participating residues in 5-HT_3R models built on the basal structure of AChBP does not allow 5-HT binding to the crucial E129 and W183 residues simultaneously. Here, we address these discrepancies and apply a dynamic receptor model. The activation process is modelled by stepwise rotations of the subunits. This is suggested by the activated structure of nicotinic receptor [2]. Moreover, the conformational changes of loop C of AChBP upon binding of agonists [12] (Figure 1) can also be modelled by anticlockwise rotation of the principal subunit. We analyse the docking of ligands with different efficacies to three 5-HT_3R models with different rotations and look for binding interactions distinctive for agonists. They contain ligand pairs whose efficacies are affected by structural modifications. We model human heteromeric 5-HT_{3AB}Rs resembling native 5-HT_3Rs functionally more than 5-HT_{3A}Rs [26]. Further, the comparison of human 5-HT_3R subunits A, B, C, and E in alignment underlines the importance of some crucial residues in binding and activation.

Methods

Receptor modelling

The extracellular regions of homopentameric human 5-HT_3Rs were built based on the crystal structure of AChBP from the snail *Lymnaea stagnalis* (PDB entry: 1I9B). The sequences of 5-HT_3R A, B, C, E subunits are from the Protein Information Resource [27]: NF00115388, NF00114949, NF00866415 and NF01471614, respectively. Multiple sequence alignments of their extracellular regions and AChBP were performed by 'ClustalW' using default parameters [28]. Based on this alignment, homology-model building of 5-HT_{3A}R and 5-HT_{3B}R subunits was carried out using the 'Nest' and 'Loopy' facility of the Jackal protein structure modeling package. 'Nest' predicts the experimental dihedral angles chi1 within an error range of 20° for 94% of protein side chains [29]. Protein loop predictions for amino acid insertions and deletion were done by 'Loopy' [30]. Heterodimeric units of the pentamer were built on the basis of crystal structure data to reach minimal root mean standard deviation (RMSD) between the matched monomers. Further refinements of the resulting dimers were carried out by the Sybyl 6.6 program (Tripos Inc., St. Louis, MO) on a Silicon Graphics Octane workstation under the Irix 6.5 operating system. The all-atom model was allowed to relax during a short molecular dynamics run (1000 fs) using constraints for backbone atoms not allowing distortions of the backbone. Finally, the entire structures were fully minimized without any restriction until the maximum derivative was less than 0.050 kcal/mol Å. Gasteiger-Hückel partial charges were applied during the calculations. Models were also built with rotated subunit A. Rotation was performed around an axis at the pseudo-symmetry center of subunit A. Stepwise rotations were −5° and −10° clockwise as well as 5°, 10°, and 15° anticlockwise. Their dimers with unchanged B subunit were energy-minimized by the same process as described above for the unrotated dimers. The quality of the model was verified using 'Procheck', as compared with well-refined structures at the same resolution [31]. Procheck showed that only 0.5% of the bonds were in the disallowed region of the Ramachandran plot. This supports that the structural properties of the 5-HT_{3AB}R model fit within the majority of the PDB. Intra- and interface H-bonds were analysed by HBPLUS v 3.0, a hydrogen bond calculation program, the algorithm of which involves finding the positions of the hydrogen atoms and calculating the hydrogen bonds [32]. The program VOIDOO [33] was used to calculate the volumes of the binding cavities for each protein. A rolling probe with the radius of 1.4 Å on a 0.75 Å grid was used for the calculation of cavity volume. Ligand volumes were calculated by Molcad as implemented in Sybyl using the Connolly molecular surface [34]. Non-local energies of rotated dimers were obtained by ANOLEA [35]. The 'non-local environment' of one heavy

atom is defined as all the heavy atoms, within an Euclidean distance of 7 Å belonging to an amino acid farther than 11 residues in the chain or belonging to another chain. All these atoms are included in the calculation of non-local interaction energies. The distances between atoms are calculated and the corresponding energy values are taken from the energy functions of the atomic mean force potential.

Ligand docking

AutoDock 3.0 [36] was applied for docking calculations, using the Lamarckian genetic algorithm (LGA) and the 'pseudo-Solis and Wets' (pSW) methods. AutoDock calculates the free energy of binding in solvent using a scoring function, which was parameterized on experimental data of inhibition constants. The parameters included in Autodock are based on the 'Assisted Model Building with Energy Refinement' (AMBER) force field [37]. Gasteiger–Hückel partial charges were applied both for ligands and proteins. Solvation parameters were added to the protein coordinate file and the ligand torsions were defined using the 'Addsol' and 'Autotors' utilities, respectively, in Autodock 3.0. The atomic affinity grids were prepared with 0.375 Å spacing using the Autogrid program for the whole target in a preliminary run and for a $15 \times 15 \times 22.5$ Å box around the interface of subunits in other cases. Random starting positions, orientations and torsions (for flexible bonds) were used for the ligands. Each docking run consisted of 100 cycles. The number of evaluations was set to 1.5 million. Final structures with RMSD less than 1.5 Å were considered to belong to the same cluster. Docking frequencies are expressed in % of 100 docking cycles. The structures with low energies and high frequencies of docking were examined.

Results

Homology modelling of 5-HT_{3AB}Rs and subunit rotation

Figure 2 shows the sequences of human 5-HT_3R subunits A, B, C and E aligned with AChBP. The N-terminal regions of subunits A and B have 24% and 22% homology with AChBP, respectively, while they have 37–42% homology with each other. Homology modelling of heteromeric 5-HT_{3AB}Rs results in two kinds of interfaces. Interface AB has a binding cavity under loop C (Figure 3). This is similar to that in 5-HT_{3A}R models [18] since loops A–C belong to the same principal subunit A. However, loop C is not long enough to bridge the gap at interface BA and to form a similar binding cavity. This is probably due to the fact that loops C of non-A subunits contain less amino acids than subunit A (Figure 2). The hydrophobic binding cavity is behind a hydrophilic vestibule separated by W183 ([17, 18] and see in an animation later).

Rotation of the principal subunit A was performed stepwise by 5°. Anticlockwise rotation results in a gradual closure while clockwise rotation leads to opening of loop C as a lid on the hydrophobic cavity. Table 1 shows that anticlockwise rotation leads to decreasing volumes of this cavity. Attractive interactions predominate along the AB interface during rotation between −10° and +10° (Table 1). Closure of the cavity at +15° starts to develop repulsive interactions (Table 1) which might then contribute to the restoration of the cavity. Three receptor 'rotamers' were analysed subsequently. The non-rotated heteromer has been called 5-HT_{3AB}R°. The direction of loop C after clockwise rotation by −10° is similar to its direction in ligand-free AChBP [12]. Therefore this model, called 5-$HT_{3AB}R^-$ and applied for docking, is considered to represent ligand-free 5-HT_{3AB}Rs. Anticlockwise rotation of 5-HT_{3AB}R° by 5° and 10° did not essentially affect docking of 5-HT (data not shown). However, about +15° of rotation eliminated the hydrophobic cleft and affected the docking of agonists. Therefore the 5-$HT_{3AB}R^+$ rotated by 15° has been applied for comparative docking. Figure 3 illustrates the relative movement of loops A–C in 5-HT_{3AB}R° into A′–C′ of 5-$HT_{3AB}R^+$ following anticlockwise rotation. Loop C gets closer to loops D and E while loops A and B, which are closer to the rotation centre, hardly move. Hydrogen bonds in the AB interface were analysed in models 5-$HT_{3AB}R^+$, 5-HT_{3AB}R° and 5-$HT_{3AB}R^-$. Table 2 summarises the distances of hydrogen bonding heteroatoms. The large number of possible interactions between the side chains (SS in Table 2) should be noted. The backbone carbonyl of the

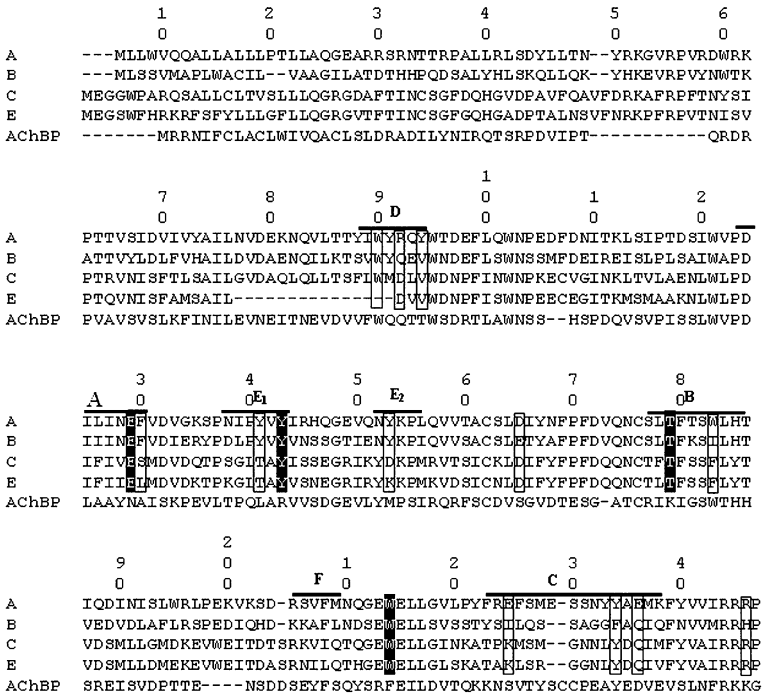

Figure 2. Alignment of the extracellular regions of human 5-HT_3R subunits A, B, C and E with AChBP. Sequence numbering of murine 5-HT_{3A}Rs is indicated for convenience. The bars show segments of loops A–F within a distance of 6 Å around the ligands docked. Subunit D does not contain an N-terminal extracellular region [9]. Residues conserved specifically in 5-HT_3Rs are in black boxes while others with crucial differences are in white boxes. W214 is conserved in Cys-loop cation channels. W214Y eliminated ligand binding and activation in correctly assembled 5-HT_{3A}Rs [47] showing its coupling role to the cation channel.

Table 1. The effect of subunit rotation on the volume of the hydrophobic binding cavity and molecular volumes of the ligands docked.

Subunit rotation (deg)	V_{cavity}[a] (Å^3)	Non-local energy (E/kT units)[b]	Ligand	$V_{Connolly}$[c] (Å^3)
			AQPA	282.3
−10	223.6	−1836	BQPA	323.8
−5	125.2	−1874	CPBG	193.8
0	108.2	−1878	Lerisetron	304.5
5	103.9	−1878	NAL	261.3
10	47.0	−1844	5-HT	178.8
15	d	+889	SR 57227	208.1

[a]Volume of the hydrophobic cavity at AB subunit interfaces. Note that it does not include the hydrophilic vestibule.
[b]Non-local energies of subunit dimers are calculated by ANOLEA [35] (kT: Boltzmann constant and absolute temperature).
[c]Molecular volumes are defined by the solvent accessible surface of ligands [34].
[d]No cavity found.

crucial W183, the side chains of Y143, Y153 in loop E [18] and of Y234 in loop C participate in multiple hydrogen bonds of 5-HT_{3AB}R° (bold in Table 2). The last column in Table 2 indicates changes in hydrogen bonds expressed in interatomic distances. Since subunit rotation results in closure of the binding cleft, the hydrogen bonding network becomes stronger. The dashed lines in Figure 4a and b demonstrate different networks of possible important hydrogen bonds around the binding cleft in 5-HT_{3AB}R° and in 5-$HT_{3AB}R^+$, respectively.

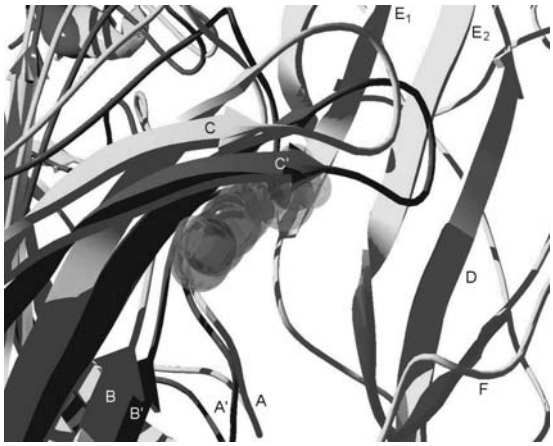

Figure 3. The binding cavity of the heteromeric 5-HT_{3AB}R models is indicated before (light) and after (dark) anticlockwise rotation of subunit A of 5-HT_{3AB}R° by +15° into 5-$HT_{3AB}R^{+}$. The rotated loops are labelled with A′–C′. The position of 5-HT docking to 5-HT_{3AB}R° is indicated.

Docking of 5-HT_3R ligands to 5-HT_{3AB}Rs with clockwise rotation has no pharmacological selectivity

Figure 5 shows the structures of 5-HT_3R ligands used for docking. SR 57227 is a full agonist [38], while *m*-chlorophenylbiguanide (CPBG) displayed partial [39] or full agonist efficacies [40] depending on the 5-HT_3R functional test. Lerisetron is an antagonist, while replacement of its N-benzyl substituent for an allyl group results in NAL, a partial agonist of 5-HT_3Rs [41]. The aryl-quinolinyl-piperazine is a full agonist (AQPA), while saturation and bicyclic extension of its phenyl ring leads to BQPA (Figure 5), a 5-HT_3R antagonist [42].

All ligands get docked into the binding site of 5-$HT_{3AB}R^{-}$ which has a hydrophilic vestibule

Table 2. Hydrogen bonding in the subunit interface AB of the heteromeric 5-$HT_{3AB}R^{o}$ model (0^{o}) after clockwise (-10^{o}) and anticlockwise ($+15^{o}$) rotation.

B subunit			A subunit			Distances (Å)				
aa		Atom	aa		Atom	Interaction	-10^{o}	0^{o}	$+15^{o}$	
E	112	O	R	58	N	MS	9.25	7.98	3.08	↑
		O	T	186	O	SS	9.37	5.28	3.16	↑
		O	Q	188	O	SS	12.31	8.35	3.04	↑
		O	N	232	N	SS	10.97	7.55	3.18	↑
S	114	O	H	185	N	SS	2.71	3.63	3.17	≈
		O	T	186	N	SM	7.97	5.97	3.17	↑
		O	D	189	O	SS	7.52	5.16	3.54	↑
		O	H	185	N	MS	5.29	4.51	3.25	↑
		N	D	189	O	MS	9.04	6.80	2.67	↑
D	138	O	**W**	**183**	N	SS	4.18	3.14	5.20	≈
Y	**141**	O	D	124	O	SS	8.58	5.42	3.11	↑
Y	**143**	O	**W**	**183**	O	SM	2.53	2.97	10.71	↓
		O	L	184	O	SM	4.67	3.32	7.52	↑↓
		O	**Y**	**234**	O	SS	6.07	3.35	9.90	↑↓
		O	T	186	O	SS	10.72	8.02	3.17	↑
		O	N	232	N	SS	13.20	10.52	2.75	↑
E	151	O	S	230	O	MS	11.44	7.70	3.12	↑
		O	S	230	O	SS	9.50	6.64	3.28	↑
Y	**153**	O	**W**	**183**	O	SM	4.67	3.34	6.43	↑↓
		O	F	226	O	SM	10.98	8.27	3.32	↑
		N	S	230	O	MS	11.52	8.52	3.28	↑
E	213	O	K	81	O	SM	4.81	3.40	7.23	↑↓

Interatomic distances are expressed in Å. Interaction is considered to take place if heteroatomic distances are less than 4 Å and bond angles (H-bond donor–acceptor–neighbour atom of the acceptor) are greater than 90°. Interactions between side chains (S) of amino acids (aa) and/or the main chain (M) are indicated. Amino acids which have been shown to affect 5-HT_3R function are labelled bold. Signs in the last column: rotation results in stronger (↑) or weaker (↓) hydrogen bonds, bidirectional changes (↑↓), or no significant change (≈).

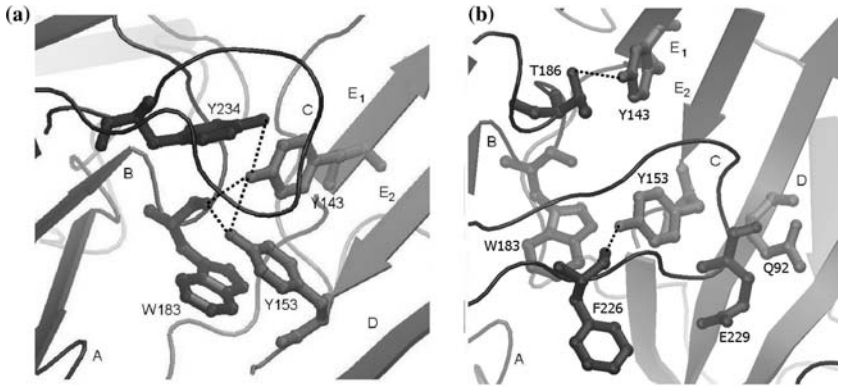

Figure 4. Network of possible AB interface hydrogen bonds in the binding cavity of 5-HT_{3AB}Rs (a) in 5-$HT_{3AB}R^{\circ}$ and (b) in 5-$HT_{3AB}R^{+}$ after anticlockwise rotation of subunit A by +15°. Dashed lines indicate hydrogen bonds based on data in Table 2.

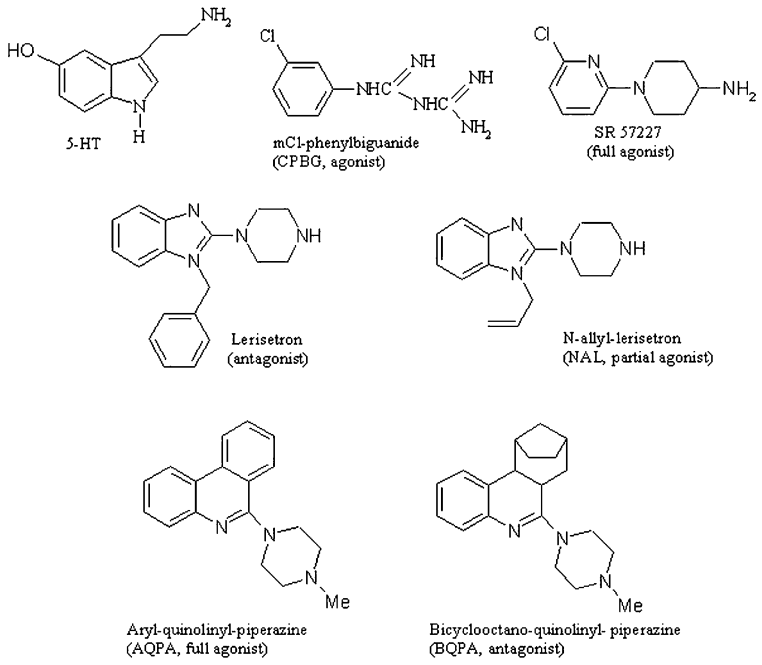

Figure 5. Chemical structures of ligands with different efficacies used for docking with the rotated 5-HT_{3AB}R models.

(N128, E129, T179, T181, E236) and a hydrophobic/aromatic cleft (W90, Y143, Y153, W183, Y234) as characterised for 5-HT_{3A}Rs [17, 18]. It is remarkable that 5-HT was docked to 5-$HT_{3AB}R^{-}$ with lowest energy (−8.81 kcal/mol) predominantly (70% of the dockings) according to Figure 6a. 5-HT is in binding distance only with residues of the principal subunit A. Hydrogen bonds can be formed between the 5-OH group and T181 as well as between the indole nitrogen atom and the carboxylic group of E236. The ammonium group of 5-HT is in hydrogen bonding distance to the backbone carbonyl group of W183 (Figure 6a). All ligands including the antagonists were docked to 5-$HT_{3AB}R^{-}$ with lowest energy and highest frequency in maximal overlap with 5-HT. Figure 7 shows this overlap for the agonists. The respective data for the docking frequencies and energies are for CPBG: 12%, −10.10 kcal/mol; SR 57227: 51%, −7.59 kcal/mol; AQPA: 72%, −14.85 kcal/mol; and NAL: 54%, −11.10 kcal/mol. The ammonium groups of all agonists were also in

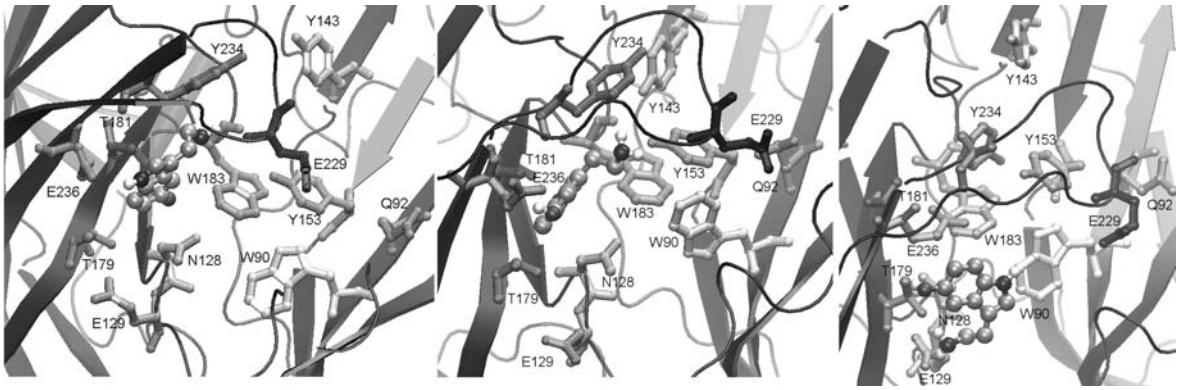

Figure 6. Docking of 5-HT to 5-$HT_{3AB}R$ models. (a) Clockwise rotation (5-$HT_{3AB}R^{-}$), (b) no rotation (5-$HT_{3AB}R°$) and (c) anticlockwise rotation (5-$HT_{3AB}R^{+}$).

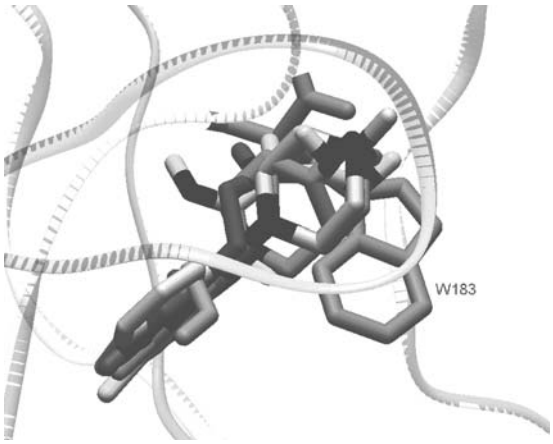

Figure 7. Docking of 5-HT_3R agonists (CPBG, SR 57227, NAL and AQPA) to 5-$HT_{3AB}R^{-}$. N atoms of the agonists are black. Note that the ammonium groups are in hydrogen bonding distance to the carbonyl group of W183. Predominant docking of the antagonists (lerisetron and BQPA) and their ammonium groups are overlapping with those of the agonists but not shown for clarity.

hydrogen bonding distance to the backbone carbonyl group of W183. Consequently, ligand docking to the 5-$HT_{3AB}R^{-}$ model with the ligand-free, open binding cavity of 5-HT_3Rs does not discriminate between the interactions of agonists and antagonists. These predominant interactions are analogous with the binding of the ammonium ion of nicotinic agonists to the backbone carbonyl group of the corresponding W143 in AChBP [12]. Moreover, the conservative D124 is in hydrogen bonding distance with the backbone amide group of W183 (not shown). Hydrogen bonding between the corresponding D85 and W143 in AChBP has been demonstrated to contribute to the charge compensation of the ammonium ions of nicotinic agonists [12]. These agreements support our subsequent selection from multiple docking in 5-$HT_{3AB}R$ rotamers with closer binding cavities.

Anticlockwise rotation of 5-HT_{3AB}Rs leads to docking selectivity for agonists versus antagonists

Figure 6b shows 5-HT docking in 5-$HT_{3AB}R°$ with lowest energy (−11.76 kcal/mol). Its ammonium group is intercalated between W183 in loop B and Y234 in loop C with π–cation–π interaction while the 5-OH group is hydrogen bonded to E236 in the hydrophilic pocket. In contrast, 5-HT cannot enter into the hydrophobic cleft of 5-$HT_{3AB}R^{-}$ and stays in the vestibule. Figure 6c shows its most frequent docking position with second lowest energy (37%, −10.86 kcal/mol). The ammonium group forms an ion pair with the crucial E129 in loop A while the 5-OH group is hydrogen bonded to T179 or N128.

Figure 8a shows docking of SR 57227 to 5-$HT_{3AB}R°$ with lowest energy and highest frequency (−7.73 kcal/mol and 50%). Its primary amino group also fits between W183 and Y234 while its other N atoms can interact with E236 and N128. Figure 8b demonstrates docking of SR 57227 to 5-$HT_{3AB}R^{+}$ with second lowest energy (−6.56 kcal/mol). The tertiary nitrogen of SR 57227 was hydrogen bonded with N128 or T179 and its heteroaromatic ring is close to E129. It may be mentioned that the structure with lowest energy (−6.66 kcal/mol with 56%) was docked in a similar position, but its amino group was hydrogen bonded to the backbone oxygen of E236.

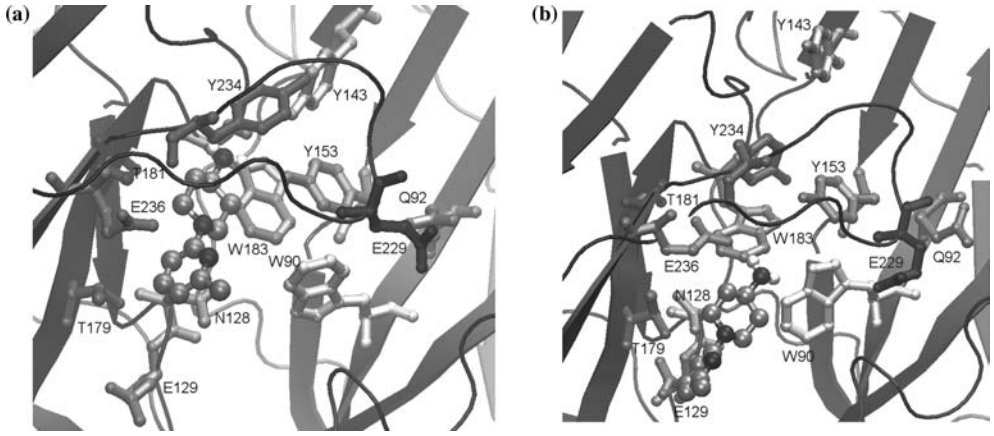

Figure 8. Docking of SR 57227 to 5-$HT_{3AB}R°$ (a) and 5-$HT_{3AB}R^+$ (b).

Docking of CPBG to 5-$HT_{3AB}R°$ resulted in four different binding positions with nearly equal energies. All of them produce electrostatic interactions with E236, while the positions of the aromatic ring of CPBG differ. Figure 9a shows docking where the chlorophenyl group is close to W90 (−7.13 kcal/mol and 15%). The external end of the guanidinium group is in cation–π interaction (W183 and Y234) while the internal end can bind to T181 and E236. Figure 9b demonstrates CPBG docking to 5-$HT_{3AB}R^+$ with lowest energy (−9.84 kcal/mol). Its guanidine stayed in the hydrophilic pocket at N128, T179 and E236. Notably, CPBG – unlike 5-HT – did not show interaction with E129, in agreement with the finding that mutations E129D/N affected 5-HT, but not CPBG binding and activation of 5-HT_{3A}Rs [24].

The most frequent docking position of the full agonist AQPA to 5-$HT_{3AB}R°$ with second energy (52% and −8.84 kcal/mol) in Figure 10a shows again that the distal ammonium is intercalated between W183 and Y234. Its antagonist derivative BQPA was docked most frequently (60% with −12.28 kcal/mol) in an almost identical position (not shown in Figure 10a for clarity). Its bulky bicyclic ring (replacing the left anellated phenyl ring in Figure 10a) might hinder the closing approach of loop C during anticlockwise rotation. Consequently, most frequent docking of the antagonist BQPA to 5-$HT_{3AB}R^+$ with lowest energy (55% with −10.84 kcal/mol) stayed in the vestibule (Figure 10b) with no reasonable binding interaction. In contrast, most frequent docking of the agonist AQPA to 5-$HT_{3AB}R^+$ (37% with

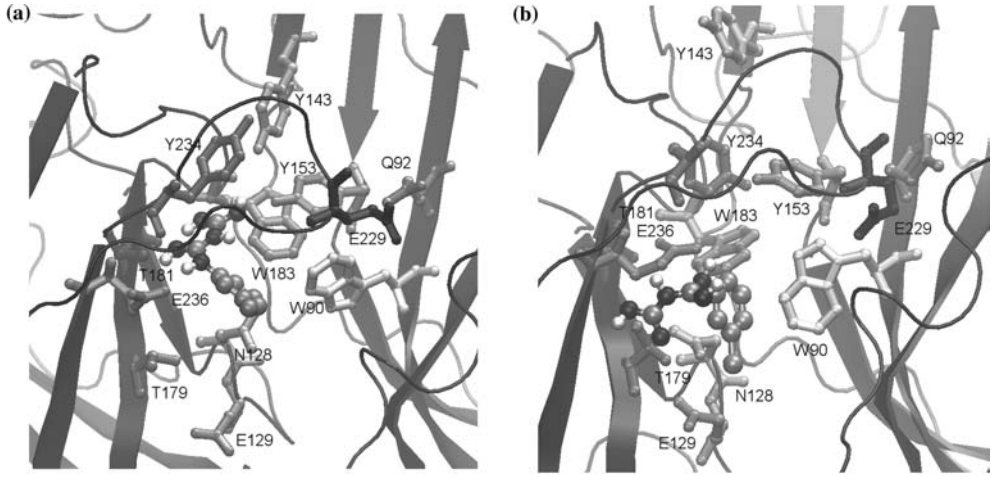

Figure 9. Docking of CPBG to 5-$HT_{3AB}R°$ (a) and 5-$HT_{3AB}R^+$ (b).

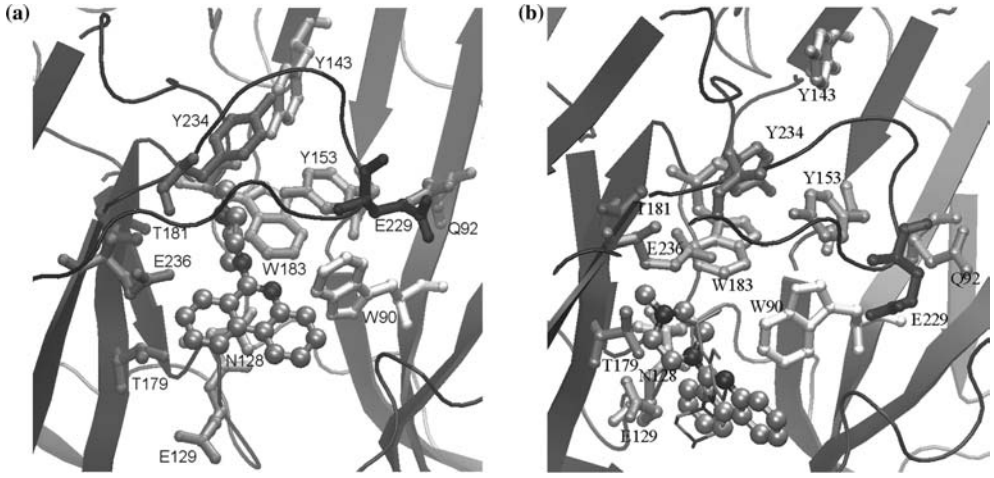

Figure 10. Docking of the agonist AQPA to 5-$HT_{3AB}R°$ (a) and 5-$HT_{3AB}R^+$ (b). Figure 10b also shows docking of the antagonist BQPA in thin.

−8.59 kcal/mol, second energy) shows the opposite position in Figure 10b, its basic piperazine ring can interact with N128 and E129, T179 and E236 in the hydrophilic vestibule. These docking patterns suggest that activation is associated with tight closure of loop C and rebinding of agonists in the hydrophilic vestibule.

Most frequent docking of the partial agonist derivative of lerisetron NAL to 5-$HT_{3AB}R°$ with lowest energy (47% and −11.24 kcal/mol) shows that the tertiary nitrogen atoms are in the hydrophilic vestibule at E236, while the distal piperazine ammonium ion is in π–cation–π interaction with W183 and Y234 again (Figure 11a). Remarkably, interactions of this distal ammonium with Y143 and Y153 (closely situated in Figure 11a) have been demonstrated [41]. Most frequent docking of the antagonist lerisetron to 5-$HT_{3AB}R°$ (27% with −12.50 kcal/mol) was in opposite position (not shown in Figure 11a for clarity), with the benzyl group intercalated between W183 and Y234, while the distal ammonium group formed an ion pair with E236. On the other hand, most frequent docking (50% with −9.72 kcal/mol) of the partial agonist NAL to 5-$HT_{3AB}R^+$ (Figure 11b) indicates that the piperazine ring was in the hydrophilic pocket surrounded by N128, T179 and E236 while the heteroaromatic ring is at E129. In contrast, docking of the antagonist lerisetron to 5-$HT_{3AB}R^+$ with lowest energy (−10.62 kcal/mol

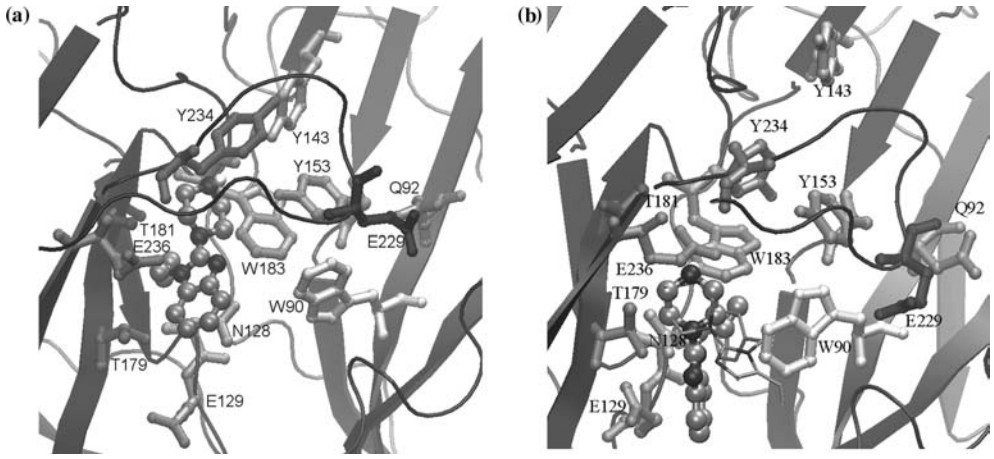

Figure 11. Docking of the partial agonist NAL to 5-$HT_{3AB}R°$ (a) and 5-$HT_{3AB}R^+$ (b). Figure 11b also shows docking of the antagonist lerisetron in thin.

with 23%) is far away from E129, close to W90, although the piperazine ring was similarly nested in the hydrophilic pocket (Figure 11b). Interestingly, the interaction of the benzimidazole group with W90 was demonstrated by point mutations W90F/Y [43] in agreement with their proximity in Figure 11b. In summary, ammonium groups of the agonists seem to interact with the backbone carbonyl of W183 in open 5-$HT_{3AB}R^{-}$, then they are intercalated between W183 and Y234 in 5-$HT_{3AB}R^{\circ}$. Finally, extensive anticlockwise rotation of loop C to form closed 5-$HT_{3AB}R^{+}$ might be associated with turning of the agonists from the hydrophobic cleft towards E129 in the hydrophilic vestibule.

The conformational changes of the 5-$HT_{3AB}R$ homology model upon anticlockwise rotation between -10° and $+15^{\circ}$ together with the predominant docking conformations of 5-HT have been built into an animation which is accessible on our homepage via http://www.chemres.hu/IBC/molpharm/5ht3.avi. The first part of this animation demonstrates the possible transformation of the water-accessible surface around the binding cavity with the closure of loop C and shifts in the docking positions of 5-HT. The second part shows possible interactions of 5-HT in the interface and movements of some amino acid residues such as W90, Y153 and Y234 that accompany subunit rotation. Of particular interest is the reversible insertion of Y153 between W183 and Y234 interrupting the β-strand of loop E, although it belongs to the non-rotated subunit B. It is homologous to L118 of α_7 nicotinic receptors which has been found the most flexible in molecular dynamics simulation of activation [44]. They support the crucial roles of Y153 and Y234 in agonist binding and activation of human 5-HT_3Rs [21].

Discussion

The crystal structure of AChBP together with homology modelling allows us to analyse interface interactions at the binding sites of Cys-loop ionotropic receptors. Molecular dynamics simulation has suggested asymmetric interface motions shrinking the binding site of a homomeric α_7 nicotinic receptor model [44]. By docking ligands of different efficacies into crystal structure-based receptor models we might find binding interactions distinctive for agonists versus antagonists. However, the emerging models of receptor activation have serious limitations because (1) moderate sequence homology leads to interaction artefacts and (2) the model is static, unable to consider different states of the ionophore. We address the second problem by a dynamic receptor model with differential rotation of the subunits. Anticlockwise rotation of the principal A subunits of 5-HT_{3AB}Rs mimics well the conformational change of loop C of AChBP upon binding of nicotinic agonists [12].

Putative roles of 5-HT_{3A}R residues

The principal component of 5-HT_3Rs is the 5-HT_{3A}R subunit. The roles of several mutated residues have been demonstrated in ligand binding and in ionophore function of homomeric 5-HT_{3A}Rs. Subunits B and C do not form functional channels by themselves but they modulate 5-HT_3R function [26, 45]. Further subunits D and E have also been cloned recently [8, 9] but their contributions to ionophore activity of 5-HT_3Rs are not known. It is informative to compare the effects of point mutations and the present modelling, based on the alignment of about 180 Cys-loop receptor protein sequences found in the PDB (data not shown) and those in Figure 2 as follows.

Mutations of W90, a conserved aromatic residue, affected the binding of antagonists and activation of 5-HT_{3A}Rs [46, 47], in agreement with receptor docking along W90 in loop D [18]. In contrast, 5-HT binding was affected predominantly by R92A [46]. We compared homomeric 5-HT_{3A}Rs containing R92 with heteromeric 5-HT_{3AB}Rs having Q92. Following anticlockwise rotation, E229 in loop C approaches Q92 in loop D of 5-HT_{3AB}Rs (Figure 6a–c). The facing ionic groups of E229 and R92 in 5-HT_{3A}Rs [18] come even closer to each other during rotation (not shown). Consequently, activation of 5-HT_{3A}Rs seems to be facilitated by a salt bridge of these residues.

Mutations E129 and F130 in loop A affect binding and activation of 5-HT_{3A}Rs for 5-HT, but not for CPBG [24, 25]. E129 is conserved in 5-HT_3R subunits while an asparagine (N) residue is conserved in the aligned position of most other

Cys-loop receptors. Yet, mutations E129N and E129D decreased ligand binding and activation by 5-HT [24]. Ion pairing of 5-HT with E129 in 5-$HT_{3AB}R^+$ (Figure 6c) is in agreement with anionic E129 required for activation. Further E129Q 5-HT_{3A}Rs turn CPBG into a low affinity antagonist [24]. All these data show specific roles of the carboxylate anion of E129 in 5-HT_3R activation. The non-conserved F130 is aligned with nonpolar residues, mainly alanine in other Cys-loop receptors. Thus, it is difficult to attribute a binding role to F130 but it might transmit activation via loop A such as mutations F130N/Y of 5-HT_{3A}Rs [25]. Tyrosines Y141, Y143 and Y153 in loop E are present in both human A and B subunits but they are not conserved in the superfamily. Their mutations affect the binding of antagonists and activation of 5-HT_{3A}Rs [20, 21]. Accordingly, these tyrosines participated in docking of several antagonists [18] and in the network of hydrogen bonding perturbed by rotation/activation.

W183 in loop B, a residue conserved in the Cys-loop family, has essential roles in the binding sites and/or activation of Cys-loop receptors such as AChBP [12] and 5-HT_{3A}Rs [47]. 5-HT_3R activation by agonists [48] as well as docking to 5-$HT_{3AB}R^\circ$ support cation–π interactions with W183, while antagonists were docked with their aromatic rings in π–π interaction with W183 [18]. Replacements of W183 in the principal faces of non-A subunits must contribute to the lack of function of their homomeric receptors. T179 and T181 are in hydrogen bonding distances in the docking of 5-HT [17] and of other agonists to 5-$HT_{3AB}R^\circ$ and 5-$HT_{3AB}R^+$ models. Therefore T181, a non-conserved residue, and especially T179, restricted to 5-HT_3R subunits, seem to have specific roles in 5-HT_3Rs [17]. Species-different ligand binding affinities can be mainly attributed to different loops C of 5-HT_3Rs [18]. E236 participates in docking of antagonists [18], binding of agonists and/or activation of 5-HT_{3A}Rs [22]. A most conserved residue Y234, like W183, seems to participate in binding distinctive for agonist (cation–π) versus antagonist (π–π) interactions. R246 in the conserved pro-TM1 region, probably in salt bridge with D165 in the conserved Cys-loop (not shown), affects gating of 5-HT_{3A}Rs [23]. The lack of functional homomers of subunit B might be attributed to the lack of these residues.

Differential interactions of agonists and 5-HT_3R activation

The activation model of 5-HT_3Rs can be combined suitably with ligand docking because the natural agonist 5-HT is the largest, least flexible of all neurotransmitters of ligand-gated ion channels while small, flexible agonists such as acetylcholine, GABA, glycine and glutamate might be docked with more artefacts. Differential docking of ligands with different efficacies to 5-HT_3Rs supports the distinctive binding interactions of agonists versus antagonists.

Since ionophore activation seems to be associated with spatial transformations of the binding cavity, activation should be considered in terms of volumes as well. There is no straightforward correlation between ligand size and efficacy, although most 5-HT_3R antagonists have greater molecular volumes than agonists (Table 1). All ligands, irrespective of their efficacy, seem to fit in the hydrophobic cavity during docking to 5-HT_3R^- and 5-HT_3R° but their substantial fractions must remain in the greater hydrophilic vestibule. Antagonists are supposed to stay there since their greater size does not allow proper transformations/contraction of the binding cavity or they (e.g. BQPA) cannot form reasonable interactions within the hydrophilic vestibule. In contrast, agonists appear to get docked in the contracted hydrophilic vestibule of 5-HT3R^+ in orientations different from their antagonist pairs. This suggests agonist rebinding during activation.

The following hypothesis can be formulated for the interactions leading to activation based on the common features of agonist docking. First, the hydrophilic acidic vestibule of the 5-HT_3R cavity containing E129 and D204 can attract and accumulate basic agonists there [18, 49]. Then the ammonium ions of all agonists are hydrogen bonded to the backbone carbonyl of W183. Hydrogen bonding by surrounding side chains of D124, Y143 and Y153 can participate in charge compensation like in AChBP [12]. Then the ammonium ions are intercalated between W183 and Y234 with π–cation–π bonding. This interaction might pull loop C, close the lid on the binding cavity and interrupt the network of hydrogen bonds there. Hydrogen bonds are perturbed mainly perpendicular to the intercalation of the ammonium groups (Y143, Y153, W183 and Y234,

in Figure 4a) while they are reorganised in a parallel manner following anticlockwise rotation into 5-$HT_{3AB}R^+$ (Figure 4b). Additional interaction of the ammonium group with Y234 might contribute to the double strength of cation–π interactions in 5-HT_{3A}Rs in comparison to that of acetylcholine in nicotinic receptors [48]. In contrast, the low potency of CPBG to activate guinea pig 5-HT_{3A}Rs [50] might be attributed to the weaker cation–π interaction with F234 there. Interestingly, tryptophane fluorescence has revealed different conformational changes in AChBP upon binding of nicotinic receptor agonists versus antagonists [51]. Molecular dynamics simulation of α_7 nicotinic receptor activation has indicated strong motions of W148 and L118 residues [44] homologous with W183 and Y153 in 5-HT_{3A}Rs, respectively. This further supports the possible role of these residues in the reorganisation of the hydrogen bond network during 5-HT_3R activation. We suppose that 5-HT bound with its 5-hydroxy side in the hydrophilic pocket might swing with its ammonium side over to E129 in the hydrophilic vestibule. Thus, the evacuated hydrophobic cleft can be closed transiently by π–π interactions of its aromatic residues.

In support of the distinct dockings, it should be mentioned that the efficacies of CPBG and 5-HT are affected by mutations of 5-HT_{3A}R differentially indicating different interactions for these agonists. CPBG unlike 5-HT has become an antagonist of E129Q 5-HT_{3A}Rs [24]. CPBG unlike 5-HT does not interact with E129 in our model. The bulky bicyclic antagonist BQPA seems to sterically hinder the closing of the binding site, that is, activation of 5-HT_3Rs. Distinct sensitivities of lerisetron derivatives for point mutations [41] can be reconciled with their distinct binding interactions.

Our activation model inevitably contains atomic interaction artefacts due to the moderate sequence homology between 5-HT_3R subunits and the AChBP template. But even this homology can result in about 80% accuracy to estimate secondary structures [11]. Consequently, several structural predictions for 5-HT_{3A}Rs have been experimentally confirmed [21, 52, 53]. We have still little information about receptor activation. However, our rotation and binding models are affected predominantly by the rotation of loop C. Other binding loops hardly move, yet intra- and inter-subunit as well as docking interactions seem to change in a functionally relevant manner during rotation. Consequently, reasonable geometric procedures and efficacy-distinctive ligand docking can lead to an activation model of 5-HT_3Rs which might be applied to the activation of other ionotropic receptors as well.

Acknowledgement

Dr. Zs. Bikádi has been supported by the QLK2-CT-2002-90436 EU project for Centre of Excellence in Biomolecular Chemistry.

References

1. Jin, R., Banke, T.G., Mayer, M.L., Traynelis, S.F. and Gouaux, E., Nat. Neurosci., 6 (2003) 803.
2. Unwin, N., Nature, 373 (1995) 37.
3. Unwin, N., FEBS Lett., 555 (2003) 91.
4. Ortells, M.O. and Lunt, G.G., Trends Neurosci., 18 (1995) 121.
5. Greenshaw, A.J. and Silverstone, P.H., Drugs, 53 (1997) 20.
6. Boess, F.G., Beroukhim, R. and Martin, I.L., J. Neurochem., 64 (1995) 1401.
7. Morales, M. and Wang, S.D., J. Neurosci., 22 (2002) 6732.
8. Karnovsky, A.M., Gotow, L.F., McKinley, D.D., Piechan, J.L., Ruble, C.L., Mills, C.J., Schellin, K.A.B., Slightom, J.L., Fitzgerald, L.R., Benjamin, C.W. and Roberts, S.L., Gene, 319 (2003) 137.
9. Niesler, B., Frank, B., Kapeller, J. and Rappold, G.A., Gene, 310 (2003) 101.
10. Brejc, K., Van Dijk, W., Klaassen, R.V., Schuurmans, M., Van Der Oost, J., Smit, A.B. and Sixma, T., Nature, 411 (2001) 269.
11. Russell, R.B., Saqi, M.A., Sayle, R.A., Bates, P.A. and Sternberg, M.J.E., J. Mol. Biol., 269 (1997) 423.
12. Celie, P.H.N., Van Rossum-Fikkert, S.E., Van Dijk, W.J., Brejc, K., Smit, A.B. and Sixma, T.K., Neuron, 41 (2004) 907.
13. Grutter, T. and Changeux, J.P., Trends Biochem. Sci., 26 (2001) 459.
14. Cromer, B.A., Morton, C.J. and Parker, M.W., Trends Biochem. Sci., 27 (2002) 280.
15. Laube, B., Maksay, G., Schemm, R. and Betz, H., Trends Pharmacol. Sci., 23 (2002) 519.
16. Costa, V., Nistri, A., Cavalli, A. and Carloni, P., Br. J. Pharmacol., 140 (2003) 921.
17. Reeves, D.S., Sayed, M.F.R., Chau, P.L., Price, K.L. and Lummis, S.C.R., Biophys. J., 84 (2003) 2338.
18. Maksay, G., Bikádi, Zs. and Simonyi, M., J. Receptors Signal Transduct., 23 (2003) 255.
19. Reeves, D.C. and Lummis, S.C.R., Mol. Membrane Biol., 19 (2002) 11.
20. Venkataraman, P., Venkatachalan, S.P., Joshi, P.R., Muthalagi, M. and Schulte, M.K., BMC Biochem., 3 (2002) 15.

21. Beene, D.L., Price, K.L., Lester, H.A., Dougherty, D.A. and Lummis, S.C.R., J. Neurosci., 24 (2004) 9097.
22. Schreiter, C., Hovius, R., Costioli, M., Pick, H., Kellenberger, S., Schild, L. and Vogel, H., J. Biol. Chem., 278 (2003) 22709.
23. Hu, X.Q., Zhang, L., Stewart, R.R. and Weight, F.F., J. Biol. Chem., 278 (2003) 46583.
24. Boess, F.G., Steward, L.J., Steele, J.A., Liu, D., Reid, J., Glencorse, T.A. and Martin, I.L., Neuropharmacology, 36 (1997) 637.
25. Steward, L.J., Boess, F.G., Steele, J.A., Liu, D., Wong, N. and Martin, I.L., Mol. Pharmacol., 57 (2000) 1249.
26. Davies, P.A., Pistis, M., Hanna, M.C., Peters, J.A., Lambert, J.L., Hales, T.G. and Kirkness, E.F., Nature, 397 (1999) 359.
27. Wu, C.H., Huang, H., Arminski, L., Alvear, J.C., Chen, Y., Hu, Z.Z., Ledley, R.S., Lewis, C., Mewes, H.W., Orcutt, B.C., Suzek, B.E., Tsugita, A., Vinayaga, C.R., Yeh, L.S.L., Zhang, J. and Barker, W.C., Nucleic Acids Res., 30 (2002) 35.
28. Thompson, J.D., Higgins, D.G. and Ibson, T.J., Nucleic Acids Res., 22 (1994) 4673.
29. Xiang, Z. and Honig, B., J. Mol. Biol., 311 (2001) 421.
30. Xiang, Z., Soto, C. and Honig, B., Proc. Natl. Acad. Sci. USA, 99 (2002) 7432.
31. Laskowski, R.A., MacArthur, M.W., Moss, D.S. and Thornton, J.M., J. Appl. Crystallogr., 26 (1993) 283.
32. McDonald, I.K. and Thornton, J.M., J. Mol. Biol., 238 (1994) 777.
33. Kleywegt, G.J. and Jones, T.A., Acta Crystallogr., D50 (1994) 178.
34. Connolly, M.L., Science, 221 (1983) 709.
35. Melo, F. and Feytmans, E., J. Mol. Biol., 277 (1998) 1141.
36. Morris, G.M., Goodsell, D.S., Hallaway, R.S., Huey, R., Hart, W.E., Belew, R.K. and Olson, A.J., J. Comput. Chem., 19 (1998) 1639.
37. Cornell, W.D., Cieplak, P., Bayly, C.I., Gould, I.R., Merz, K.M. Jr., Ferguson, D.M., Spellmeyer, D.C., Fox, T., Caldwell, J.W. and Kollman, P.A., J. Am. Chem. Soc., 117 (1995) 5179.
38. Bachy, A., Keane, P.E., Gozlan, H., Hamon, M., Delagne, P., Lassalle, J. and Soubrié, P., Br. J. Pharmacol., 108 (1993) 256P.
39. Kilpatrick, G.J., Butler, A., Burridge, J. and Oxford, A.W., Eur. J. Pharmacol., 182 (1990) 193.
40. Sepúlveda, M.I., Lummis, S.C.R. and Martin, I.L., Br. J. Pharmacol., 104 (1991) 536.
41. Parihar, H.S., Suryanarayanan, A., Ma, C., Joshi, P., Venkataraman, P., Schulte, M.K. and Kirschbaum, K.S., Bioorg. Med. Chem. Lett., 11 (2001) 2133.
42. Cappelli, A., Anzini, M., Vomero, S., Canullo, L., Mennuni, L., Makovec, F., Doucet, E., Hamon, M., Menziani, C., Benedetti, P.D., Bruni, G., Romero M.R., Giorgi, G. and Donati. A., J. Med. Chem., 42 (1999) 1556.
43. Venkataraman, P., Joshi, P., Venkatachalan, S.P., Muthalagi, M., Parihar, H.S., Kirschbaum, K.S. and Schulte, M.K., BMC Biochem., 3 (2002) 16.
44. Henchman, R.H., Wang, H.L., Sine, S.M., Taylor, P. and McCammon, J.A., Biophys. J., 85 (2003) 3007.
45. Dubin, A.E., Erlander, M.G., Huvar, A., Huvar, R. and Buehler, L.K., US Patent No. 6,365,370, 1999.
46. Yan, D., Schulte, M.K., Bloom, K.E. and White, M.M., J. Biol. Chem., 274 (1999) 5537.
47. Spier, A.D. and Lummis, S.C.R., J. Biol. Chem., 275 (2000) 5620.
48. Beene, D.L., Brandt, G.S., Zhong, W., Zacharias, N.M., Lester, H.A. and Dougherty, D.A., Biochemistry, 41 (2002) 10262.
49. Tairi, A.P., Hovius, R., Pick, H., Blasey, H., Bernard, A., Surprenant, A., Lundström, K. and Vogel, H., Biochemistry, 37 (1998) 15850.
50. Lankiewicz, S., Lobitz, N., Wetzel, C.H.R., Rupprecht, R., Gisselmann, G. and Hatt, H., Mol. Pharmacol., 53 (1998) 202.
51. Hansen, S.B., Radic, Z., Talley, T.T., Molles, B.E., Deerinck, T., Tsigelny, I. and Taylor, P., J. Biol. Chem., 277 (2002) 41299.
52. Price, K.L. and Lummis, S.C.R., J. Biol. Chem., 279 (2004) 23294.
53. Bouzat, C., Gumilar, F., Spitzmaul, G., Wang, H.L., Rayes, D., Hansen, S.B., Taylor, P. and Sine, S.M., Nature, 430 (2004) 896.